










Surface effects on a photochromic spin-crossover iron(II) molecular switch adsorbed on highly oriented pyrolytic graphite†

Lorenzo Poggini, *^a Giacomo Londi, ^a Magdalena Milek,^b Ahmad Naim, ^c Valeria Lanzilotto, ‡^a Brunetto Cortigiani,^a Federica Bondino, ^d Elena Magnano,^d Edwige Otero,^e Philippe Sainctavit,^{e,f} Marie-Anne Arrio,^f Amélie Juhin,^f Mathieu Marchivie,^c Marat M. Khusniyarov, ^b Federico Totti, *^a Patrick Rosa ^c and Matteo Mannini ^a

Thin films of an iron(II) complex with a photochromic diarylethene-based ligand and featuring a spin-crossover behaviour have been grown by sublimation in ultra-high vacuum on highly oriented pyrolytic graphite and spectroscopically characterized through high-resolution X-ray and ultraviolet photo-emission, as well as *via* X-ray absorption. Temperature-dependent studies demonstrated that the thermally induced spin-crossover is preserved at a sub-monolayer (0.7 ML) coverage. Although the photochromic ligand *ad hoc* integrated into the complex allows the photo-switching of the spin state of the complex at room temperature both in bulk and for a thick film on highly oriented pyrolytic graphite, this photomagnetic effect is not observed in sub-monolayer deposits. *Ab initio* calculations justify this behaviour as the result of specific adsorbate–substrate interactions leading to the stabilization of the photoinactive form of the diarylethene ligand over photoactive one on the surface.

Introduction

Spin-Crossover (SCO) metal complexes are among the most attractive systems as building blocks for spintronics, data storage, and sensing devices.^{1–3} These species may commonly exist in two electronic states with different magnetic, optical, and structural properties, and can be reversibly switched by various external stimuli (pressure, temperature, light-irradiation).^{4,5} Their surface organization by sublimation processes onto different substrates, with controlled thickness

from micrometres down to sub-monolayer coverage, is crucial for forthcoming technological applications, becoming a highly attractive and flourishing research field during recent years.^{6–18}

The retention of switching capability in molecular-inorganic architectures obtained by the regular assembling of SCO molecules on conductive surfaces is a mandatory step towards their integration in hybrid devices. In particular the possibility of obtaining bistable thin films of Fe(II) SCO complexes has been suggested in several recent reports.^{19–25} Most of these studies highlighted that direct surface–adsorbate interactions can significantly modify the thermodynamics of SCO. While HOPG (Highly Oriented Pyrolytic Graphite) supported SCO systems were reported to preserve its switching capability similarly to bulk,^{23,26} sub-monolayer deposits of several Fe(II) complexes show a selective stabilization of one of the spin states in detriment of the others and loss of their original SCO behaviour when evaporated on metallic surfaces.^{7,16,27–29}

Very recently, we reported the possibility of controlling the spin state of a SCO thin film by light at room temperature. This photo-switching was observed in a 5 nm thin film of [Fe^{II}(H₂B(*pz*)₂)₂(*phen**)], **1** (where *pz* is 1-pyrazolyl and *phen** is a diarylethene functionalized phenanthroline ligand, Fig. 1a), deposited on Au(111).²⁵ The photochromic ligand allows a ligand-driven light-induced spin change (LD-LISC) effect:^{30,31} a

^aDepartment of Chemistry “Ugo Schiff” and INSTM Research Unit of Firenze, University of Firenze, I-50019 Sesto Fiorentino, Italy.

E-mail: lorenzo.poggini@unifi.it, federico.totti@unifi.it

^bDepartment of Chemistry and Pharmacy, Friedrich-Alexander University Erlangen-Nürnberg (FAU), Egerlandstr. 1, 91058 Erlangen, Germany

^cCNRS, Univ. Bordeaux, ICMCB, UMR5026, F-33600 Pessac, France

^dCNR-IOM, Laboratorio TASC, Basovizza SS-14, Km 163.5, 34149 Trieste, Italy

^eSynchrotron SOLEIL L’Orme des Merisiers Saint Aubin, BP 48 91192 Gif sur Yvette, France

^fIMPMC-UMR7590, CNRS, Sorbonne université, MNHN 4 place Jussieu, 75005 Paris, France

†Electronic supplementary information (ESI) available. See DOI: 10.1039/c9nr05947d

‡Present affiliation: Dipartimento di Chimica, Università degli Studi di Roma “La Sapienza”, Piazzale Aldo Moro 5, I-00185, Roma, Italy.

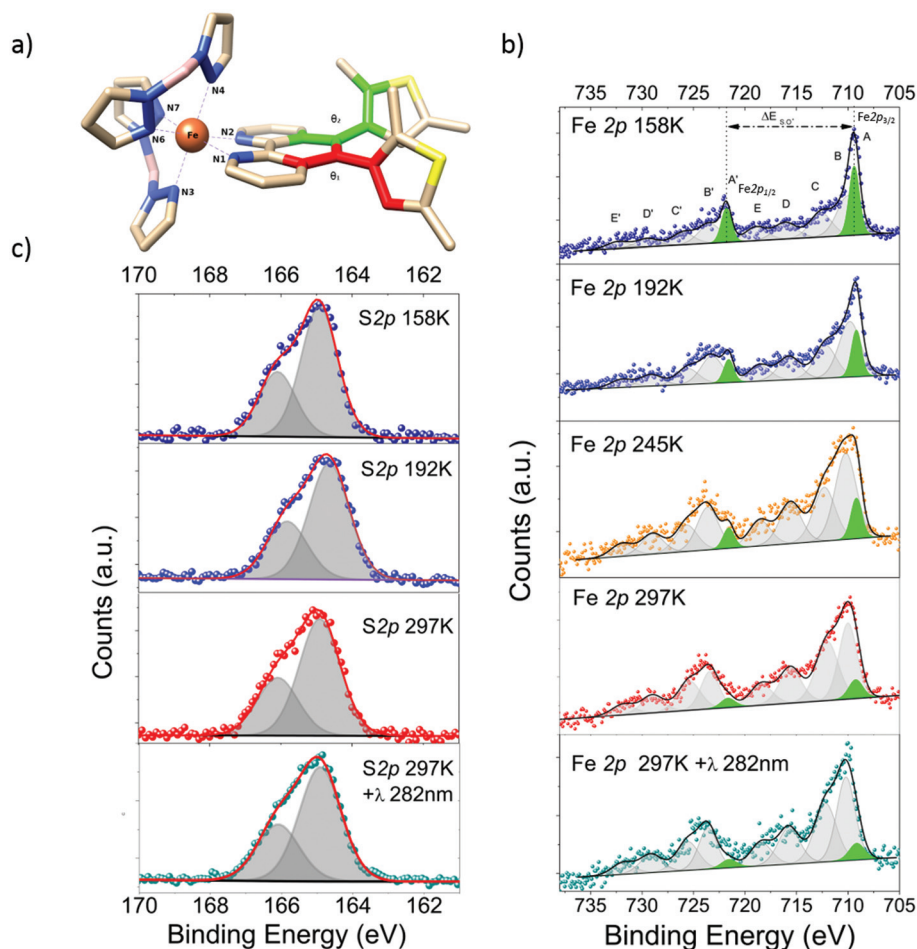


Fig. 1 (a) Optimised structure of $[\text{Fe}^{\text{II}}(\text{H}_2\text{B}(\text{pz})_2)_2\text{phen}^*]$, **1**, with nitrogen labelling used in Table S3.† In red and green are also coloured the carbon atoms defining the two dihedral angles θ_1 and θ_2 . The other carbon atoms are coloured as light brown while the sulphur ones as yellow. Hydrogen atoms have been omitted for the sake of clarity. Fe 2p (b) and S 2p (c) XPS regions for a sub-monolayer of **1** evidencing the reversibility of the SCO behavior as a function of the temperature (dark blue, blue, orange, red and cyan spectra have been acquired respectively at 158, 192, 245, 297 and 297 K after 282 nm exposure).

reversible photocyclization of the photoactive diarylethene-based ligand which remotely triggers a high-spin to low-spin crossover at the coordinated iron(II) ion.^{32,33} Accordingly to earlier reports,³⁴ this photocyclization can be observed only when the ligand maintains a specific photoactive conformation with the two aryl rings in an antiparallel orientation.

Here we move a step forward by exploring the behaviour of a sub monolayer deposit, with 0.7 monolayers (ML) of **1** sublimated in ultra-high vacuum (UHV) on HOPG substrates.

In order to investigate the chemistry and switching properties of this submonolayer deposit and to further develop the multi-technique protocol for the characterization of magnetic molecules at the nanoscale,^{35–38} we combined here high-resolution photoelectron spectroscopy (HR-XPS), high-resolution ultraviolet photoelectron spectroscopy (HR-UPS), and variable temperature X-ray absorption spectroscopy (XAS) with state-of-the-art density functional theory (DFT) modelling. This paper reports, for the first time, about surface-induced inhibition of the LD-LISC mechanism.

Results and discussion

A submonolayer (*ca.* 0.7ML) of **1** was prepared under UHV conditions by thermal sublimation from crystalline powders on HOPG. The thickness of the film has been estimated using a quartz microbalance and confirmed spectroscopically using the edge jump method from the XAS.³⁷ The substrate was cleaved in air and gently heated up to 330 K in UHV to remove possible adsorbates before the deposition. The molecular integrity on the surface was verified by an XPS-based semi-quantitative analysis (see Table S1†). Within the limits of the XPS analysis, the experimentally obtained values agree nicely with the expected stoichiometry of the pristine **1** complex. The uncertainty in the semiquantitative estimation is given by multiple factors, like the low concentration of the relative atom, the surface distribution in respect to the analyser and the estimated cross section at the given energy.³⁹ High-resolution XPS spectra of the sublimated sample on HOPG as a function of temperature and light irradiation are reported in Fig. 1

for the Fe 2p and S 2p regions (Fig. 1b and c respectively). The temperature-dependence of the line shape in the Fe 2p spectra (Fig. 1b), confirms a thermally driven SCO, which is in line with our previous results on a corresponding thin film.²⁵ The thermally induced SCO in the submonolayer on HOPG is fully reversible (Fig. S3c†). In the present case such a behaviour is evidenced by the changes observed in the line shape of the Fe 2p_{3/2} peak: in the partially LS configuration at 158 K, the Fe 2p_{3/2} peak appears narrower than in the one for HS configuration at 297 K.⁴⁰ An additional fingerprint is the energy difference ($\Delta E_{2p_{3/2}-2p_{1/2}}$) between the maxima at 2p_{3/2} and 2p_{1/2} peaks for LS and HS: $\Delta E_{2p_{3/2}-2p_{1/2}}$ is lower for LS than for HS. This reversible spin crossover can be followed using a well-established peak fitting procedure^{20,25,41} by monitoring the components (Fig. 1b) at 708.9 eV and 721.3 eV that can be directly attributed to the LS species. We notice that this thermally driven process does not involve an alteration of the *phen** ligand but it is limited to the geometrical changes of the iron coordination geometry (Fig. 1b and c), being the responsible of the ligand field alteration and, consequently, of the SCO effect.³² This can be confirmed by the unchanged S 2p signal centred at 165.0 eV in agreement with literature data (Fig. 1c).^{25,42,43}

Further tests were performed at room temperature to evaluate if this sub-monolayer deposit of **1** can be converted at room temperature *via* UV irradiation analogously to what was previously observed on a thick film.²⁵ From the direct comparison of the spectra (Fe 2p and S 2p) obtained at 297 K after UV irradiation ($\lambda = 282$ nm) with those recorded at 297 K in the dark, no significant change in the line shape can be noticed upon irradiation. The fitting of these spectra evidences that there is not any detectable UV-induced HS-to-LS spin crossover in sub-monolayers (all the details of the spectral components obtained for the Fe 2p XPS by a least square fitting procedure are reported in Table S2†). This is in contrast to successful UV-induced SCO behaviour achieved in solution,³² crystalline phase,⁴⁴ and 5 nm thick films on Au(111).²⁵ The irradiation is expected to promote the cyclization of the *phen** ligand in **1**, which takes place, when the two aryl rings are in an antiparallel orientation, from the open ligand structure (*phen*-o*) to a closed one (*phen*-c*)^{25,44} as observed in similar diarylethene systems.⁴⁵⁻⁴⁷ This modification induces the SCO behaviour at RT. We already demonstrated that XPS is sensitive to this cyclisation and to the corresponding SCO.²⁵ However, in this case, no alteration in the Fe 2p and S 2p line shapes were observed after UV exposure, thus confirming the persistence of the ligand in the open structure (*phen*-o*).²⁵ This general behaviour is also confirmed by an UPS characterization performed on the same sample (Fig. S1†). The spectra evidence contributions at -2.3 eV, -4.2 eV (shoulder), -6.5 eV, -9.4 eV, and a very broad feature centred at -12.5 eV, in line with literature reports.^{14,17,25,28} The temperature effect on the UPS spectra is visible mainly at -2.3 eV in the valence-Fermi region and at -9.4 eV in the semi-core region. However, the presence of a shoulder band in this semi-core region at 297 K can be assigned to the presence a small LS fraction of molecules at

this temperature. Upon UV irradiation, no significant energy shift is observed for the band at -2.3 eV compared to the one observed at 297 K, in contrast to what is seen for similar diarylethene system^{48,49} as well as in the case of thick films of the same complex on gold.²⁵ The UPS spectra support what was observed with XPS spectra in the Fe 2p region: after the UV exposure no ligand cyclization occurs for the diarylethene ligand. When the thermal switching occurs, a variation in the line shape is observed in line with previous reports.^{17,25,28} However, no quantitative hints on the HS/LS ratio can be easily extracted.

To follow the thermal induced spin crossover at the nanoscale, we also performed a variable temperature XAS characterization. Synchrotron-based absorption techniques are unmatched tools to analyse submonolayer deposits of bistable molecular systems, providing the required sensitivity to monitor the oxidation state,³⁵ the spin states^{15,23,35} and molecular orientation on surfaces.^{50,51} Fig. 2 displays the temperature evolution of the absorption spectrum at the L_{2,3} edges of Fe of a monolayer of **1** in the 75–300 K temperature range (while data taken at additional temperatures are reported in Fig. S2a†). We have estimated the molar fraction of the HS species by fitting the experimental XAS spectra as described in the method section achieving the plot reported in Fig. 2b. It can be noticed that **1** shows spin crossover between 75 and 300 K ($T_{1/2} = 168(15)$ K), reversible upon subsequent thermal treatments, and slightly shifted with respect to the 4 nm deposit on HOPG ($T_{1/2} = 146(8)$ K, see Fig. S2b†) and respect SCO behaviour of the bulk crystalline compound³² ($T_{1/2} = 135(5)$ K) due to a more gradual thermal driven SCO. Furthermore, the efficiency of the thermal switch in the nanostructured sample ($n_{\text{HS}} \approx 0.31(6)$ at 75 K and $\approx 0.88(4)$ at 297 K) is less than in the bulk ($n_{\text{HS}} \approx 0.11(2)$ at 75 K and $\approx 0.99(2)$ at 300 K). At lower temperatures, both soft X-ray induced excited spin state trapping (SOXIESST)^{15,41} and Light-Induced Excited State Trapping (LIESST)^{4,52} effect can be observed, the former can be directly evidenced from the analysis of the spectra evolution upon irradiation with the X-ray beam, the latter by irradiating the sample at 10 K with a laser of 660 nm wavelength. It must be stressed that SOXIESST and LIESST are phenomenologically similar, the former being caused indirectly by secondary photoelectrons, the latter being caused by direct absorption of photons.⁵³ The black spectra in Fig. S3a† has been recorded after 30 min of X-Ray irradiation to assure that the spin transition *via* SOXIESST has been completed. Only afterwards the sample has been irradiated for 1 hour with 660 nm laser diode (purple spectra in Fig. S3a†). The LS–HS conversion at low temperature is evident, with X-rays inducing partial conversion even under conditions of low photon flux (Fig. S3a†). Thermal relaxation of the photoexcited state can be monitored while increasing the temperature (Fig. 2c and Fig. S3b†) and results comparable to what was observed on a thicker film (Fig. S2c†) giving a $T_{1/2}$ of 56(3) K and 61(5) K, respectively.

Both the XPS and XAS measurements at 297 K confirmed the coexistence of LS and HS states in the monolayer deposit. XAS suggests that the HS fraction can be estimated to be $\approx 0.88(4)$,

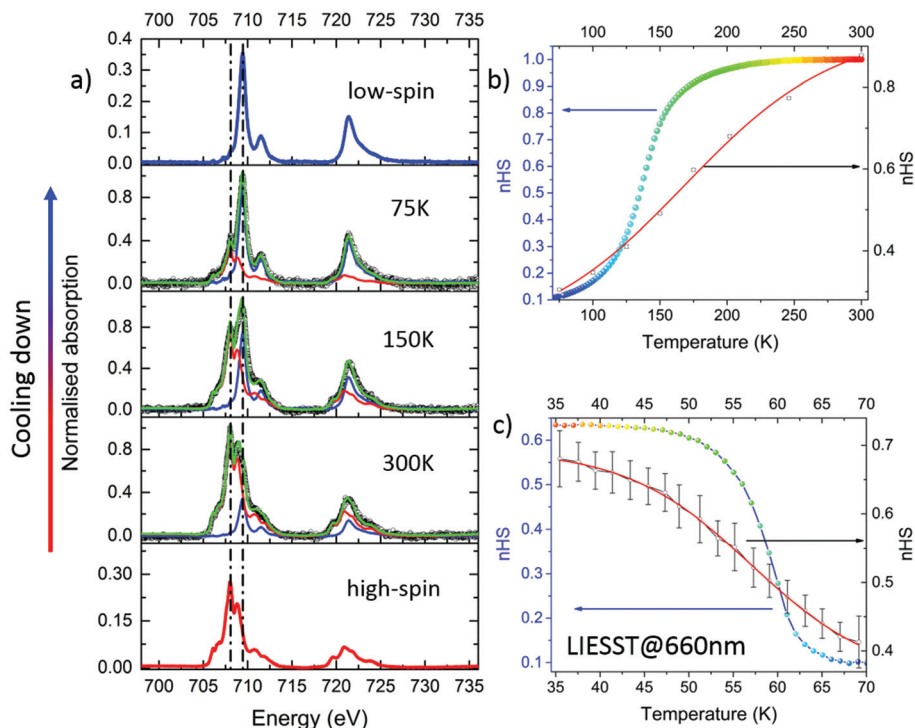


Fig. 2 (a) Temperature evolution of the normalised $\text{FeL}_{2,3}$ edge XAS spectra of a monolayer of **1** (empty black dots) along with high-spin Fe(II) and low-spin Fe(II) spectra (red line and blue, respectively and taken from ref. 15) used as reference signals for the spectral deconvolution (green lines). Broken lines are guides to the eye. (b and c) High-spin Fe(II) thermal distribution profile (empty circles) obtained from XAS spectra taken before (b) and after (c) laser light irradiation at 4 K. In (b) and (c) the red line is the fit of empty black dots by a Boltzmann distribution, giving a $T_{1/2} = 168 \pm 15$ K and $T_{1/2} = 56 \pm 3$ K respectively. The data measured for the bulk sample are reported as wide coloured dots for comparison taken from ref. 32.

deviating from what was observed on a thicker film (4 nm deposit on HOPG) where the HS fraction was 0.98 (3) (see Fig. S2b and c†). This comparison reveals the coexistence of HS ($\approx 90\%$) and LS species ($\approx 10\%$) in the 0.7 ML film at 297 K; such behaviour can be attributed to a very gradual SCO conversion in the film with a residual HS fraction at low temperature that from the XAS experiments can be estimated to be about 30% remaining at 75 K (above the occurrence of LIESST and SOXIESST). A comparison between the thermal switching of the pristine powder sample and the sublimated film, both for the 0.7ML (Fig. 2b) and for the 4 nm on HOPG (Fig. S2†), reveals that the nano-structuration has a strong effect on the compound even if a degradation of this system can be excluded for this complex, because the XPS and XAS line-shapes are in line with what expected for this family of complexes.^{15,25} These findings can result from structural distortion of the intact molecules, similar to what was previously found for other SCO systems.^{54,55}

Upon cooling from 300 to 75 K, the spectral features related to the LS- Fe(II) gained intensity as expected, while the signal due to the HS- Fe(II) weakened. Upon heating the sample back to 300 K, the initial spectrum is restored, thus confirming the full reversibility of the thermally driven switching (see Fig. S3c†).

In Fig. S4† is reported the Fe L_3 edge spectrum for 0.7 ML of **1** on HOPG irradiated with UV wavelength ($\lambda = 282$ nm) for

12 hours, compared with the one non-irradiated. The least-squares interpolation used to fit these XAS data indicates that the irradiation does not influence the spin state of the system at this coverage on HOPG, unlike on a much thicker film on $\text{Au}(111)$.²⁵

Our analysis points out that in the sub-monolayer deposit it is possible to quantitatively measure the thermal switchability of **1** that is comparable with what was observed on thicker sample (Fig. S1†). However, as evident in Fig. 2c, the switching behaviour of the thinnest film of **1** we prepared is different from that of the bulk, which we attribute to the change in entropy and enthalpy contributions respect to the bulk, due to the interaction with the surface. Similar effects have been observed also in other SCO complexes by playing on the dilution of the metal centres as well as on the crystal packing.^{54–56}

To shed some light on the absence of the diarylethene ligand cyclization upon UV irradiation when these molecules are adsorbed on HOPG we modelled the interaction of **1** with HOPG at the periodic DFT level (see Experimental part for details on the used method). We calculated four possible scenarios, including the two conformers of the ligand: a parallel conformer (par) with 2-methyl groups of two thiophenes pointing in the same direction and an antiparallel conformer (anti) with 2-methyl groups of two thiophenes pointing in opposite directions, and two possible spin states of Fe(II) : LS and HS.

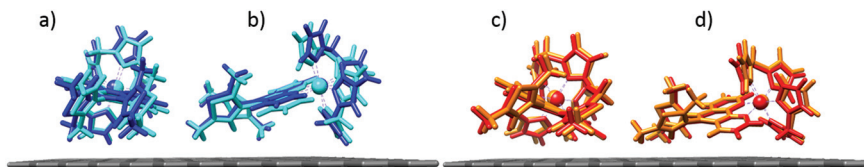


Fig. 3 Superimposed computed geometries for 1-anti-LS (blue), 1-anti-HS (cyan), 1-par-LS (red), and 1-par-HS (orange): front (left) and side (right) views. Only the topmost HOPG layer was left for the sake of clarity.⁶⁶ The view in (a) and (c) evidences the differences in the thiophenes tilting for 1-anti and 1-par; (b) and (d) panels focus on the distortions occurring on the metal centers and on H₂B(pz)₂ ligands.

The following four geometries have been optimized: 1-anti-LS, 1-par-LS, 1-anti-HS and 1-par-HS. This optimization has been carried out placing the molecules on an optimized HOPG substrate starting from a guess structure where the hydrogen atom of the pyrazolyl group pointing towards the surface was set 2 Å distant from the surface and with the phenanthroline group almost parallel to the latter.

According to the crystalline structure of **1** (see ESI Table S3†) the geometrical environment of the iron centre was conserved throughout the optimization process for all the conformers, suggesting that the deposition process on HOPG has only negligible effects on the metal ligand field. However, depending on the conformers, the thiophene groups of the diarylethene moiety rearranged their orientation differently (see dihedral angles, θ , in Table S2†). Indeed, while for 1-anti conformers the rotation of both thiophenes is substantially inhibited by the steric hindrance induced by their methyl groups, a thiophene group can rotate up to be almost parallel to the surface in the case of the 1-par conformers (see Fig. 3 and Table S2†). Such a rotation allows a stronger interaction of the complex with the surface and, indeed, both the phenanthroline ligand and the iron ion are closer to it, differently from what was observed for the 1-anti conformers. In the light of such results, rather different adsorption enthalpy, $\Delta H_{\text{abs}}^{\text{el}}$, values are, therefore, expected for the 1-par and 1-anti conformers. The adsorption enthalpy for each SCO conformer was calculated as:

$$\Delta H_{\text{ads}}^{\text{el}} = \Delta H_{\text{1@HOPG}}^{\text{el}} - (\Delta H_{\text{HOPG}}^{\text{el}} + \Delta H_{\text{1}}^{\text{el}}) \quad (1)$$

where $\Delta H_{\text{1@HOPG}}^{\text{el}}$ is the electronic enthalpy of **1** adsorbed on the HOPG surface system, while $\Delta H_{\text{HOPG}}^{\text{el}}$ and $\Delta H_{\text{1}}^{\text{el}}$ stand for the electronic enthalpy of the isolated species. Net to the entropic contributions which are expected to be similar for the two conformers and spin states, the data reported in Table 1 clearly show that the most energetically stable conformers adsorbed on HOPG are the parallel ones with a gain for $\Delta H_{\text{abs}}^{\text{el}}$

Table 1 Computed electronic adsorption enthalpies, $\Delta H_{\text{abs}}^{\text{el}}$, of the 1-par and 1-anti conformers in both HS and LS state

	$\Delta H_{\text{abs}}^{\text{el}}$ (kcal mol ⁻¹)		$\Delta H_{\text{abs}}^{\text{el}}$ (kcal mol ⁻¹)
1-par-LS	-40.59	1-par-HS	-40.12
1-anti-LS	-29.29	1-anti-HS	-28.36
ΔH_{LS}	11.30	ΔH_{HS}	11.76

of more than 11 kcal mol⁻¹ with respect to antiparallel ones. Such results can be rationalized based on the conformational rearrangements which stabilize the interaction between the HOPG surface and the π electron rich periphery of **1**, *i.e.* the phenanthroline and the thiophene groups.

Since the photo-induced mechanism occurs exclusively for the antiparallel conformers according to the Woodward-Hoffman's rules, a preferential energy-driven room temperature deposition on HOPG would lead to a preferential formation of a ML of 1-par-HS, so preventing the photocyclization and, consequently, the light-induced switching from HS to LS at room temperature. As a side remark, we also highlight that the LS conformers are still more stable, as expected, than their HS counterparts (0.47 and 0.93 kcal mol⁻¹ for the parallel and the antiparallel conformers, respectively). Density of states (DOS) were computed for both the LS and HS species in their extrapolated scenario and are reported in Fig. S1† for the 1-par conformer (the 1-anti is superimposable). The overall density profile maintains all the features present in the bulk DOS for both the LS and HS species, especially for the fingerprint valence region.²⁵ This outcome shows that the adsorption process does not induce severe changes in the whole structure, and, above all, in the sensitive iron ion ligand field but perfectly explains the origin of the quenching of the photo-switching capabilities at room temperature for this complex.

Conclusions

A spin-crossover molecular switch featuring a photochromic diarylethene-based ligand was successfully evaporated in ultra-high vacuum to form a sub-monolayer on highly oriented pyrolytic graphite (HOPG). The integrity of the complex was confirmed by high-resolution X-ray photoelectron spectroscopy, X-ray absorption spectroscopy, and density functional theory calculations flanked by ultraviolet photoelectron spectroscopy. Thermally-induced reversible switching of sub-monolayers and their photo-switching at cryogenic temperatures *via* the LIESST effect have been demonstrated while we noticed that the expected room temperature photoconversion *via* the LD-LISC effect is not occurring in the case of submonolayer deposits and this is attributed to a selective surface-driven destabilization of the photoactive antiparallel conformer of the molecular switch. Indeed, the HOPG substrate tends to stabilize a photoinactive parallel conformer leading to the loss of photoactivity of the material.

On the basis of these evidences, with this work we point out that unexpected changes or even lost of functionality of multifunctional molecules in (sub-)monolayers can be induced by surface-driven selective absorption, and at the same time, we alert the community on the peculiar role substrate-adsorbate interactions may play when dealing with bistable molecular systems on surfaces.

Experimental

Monolayer preparation

Sub-monolayers of $[\text{Fe}(\text{H}_2\text{B}(\text{pz})_2)(\text{phen}^*)]$ were prepared by thermal evaporation in UHV by heating the powder with an in-house cell. Sublimation was carried out using a resistively heated quartz crucible in UHV ($P < 5 \times 10^{-9}$ mbar) and the nominal thickness of the molecular films was measured by oscillating quartz microbalance. Before deposition, the crucible with solid was held at the sublimation temperature, *i.e.* ~ 430 K, for several hours to remove lattice solvent and any volatile contaminant. The SCO molecules were then deposited on fresh cleaved HOPG held at room temperature, by using a deposition rate of about $0.15 \text{ \AA min}^{-1}$.

HR-XPS, HR-UPS measurements

XPS and UPS experiments were performed at the BACH beamline in Elettra the Italian Synchrotron Radiation Facility in Trieste. All the experiments were carried out in a UHV chamber apparatus consisting of one chamber with a base pressure in the low end of the 10^{-9} mbar range, using X-ray synchrotron radiation at 1077.86 eV and 46 eV energies for XPS and UPS respectively, and a VG Scienta R3000 hemispherical analyser mounting a 2D-detector. The X-ray source is at 60° with respect to the analyser. XPS and UPS spectra were measured at normal emission with a fixed pass energy of 200 eV. The XPS binding energy (BE) scale was calibrated setting the C 1s photoemission peak of the HOPG single crystal slab at 284.6 eV.⁵⁸ The UPS energy ($E - E_F$) scale was calibrated subtracting both the energy used and the sample work function (obtained from XPS). In the XPS the intensity of the signal for each element corresponds to the area of the peak, calculated by standard deconvolution using for each component a mixed Gaussian (G) and Lorentzian (L) line-shapes (ratio $G = 70\%$ $L = 30\%$) and subtracting the inelastic background by means of the linear background. The stoichiometry was calculated by peak integration, using reported cross-section in literature.⁵⁹

XAS characterization

XAS spectra were acquired at the DEIMOS beamline of the SOLEIL Synchrotron Radiation Facility in Paris, France, on a UHV compatible pumped ^4He cryo-magnet.⁶⁰ All the samples were inserted into the Cromag end station, working in the 8–300 K range and equipped with optical windows for sample irradiation with a 660 nm diode. XAS spectra were measured in Total Electron Yield (TEY) detection mode to guarantee the

optimal detection sensitivity. All the characterisations were performed using a low density of photons in order to avoid radiation damage, as checked by the absence of evolution of RT spectra. Estimation of the temperature dependence of the $n\text{HS-Fe(II)}$ molar fraction of the submonolayer coverage was performed through least-squares interpolation of normalized L_3 XAS spectra with the ones of similar $[\text{Fe}(\text{H}_2\text{B}(\text{pz})_2)(\text{bipy})]^{15}$ complexes, as recorded in similar experimental conditions. The photon fluence of the 660 nm laser was 10 mW cm^{-2} on the sample. The UV irradiation of the film was performed *in situ* using a deuterium lamp (20 W) equipped with a band-pass filter ($282 \pm 5 \text{ nm}$).

DFT calculations

All the calculations were performed with CP2K 5.1 suite package⁶¹ within the DFT framework,^{62,63} using a GGA revised PBE⁶⁴ exchange–correlation functional. Nonlocal functional corrections were added in order to account for the long-range dispersion van der Waals interactions (rVV10).⁶⁵ DZVP-MOLOPT-SR (double- ζ polarized molecularly optimized at short range) basis sets were chosen for all the atomic species along conserving Goedecker–Teter–Hutter (GTH) pseudopotentials.⁶⁵ A large energy cut-off of 550 Ry was applied to the plane-wave basis set. The HOPG (001) surface was “standalone” optimized as a four-layer slabs, each layer consisting of 288 carbon atoms, according to the graphite ABAB crystalline structure. The size of the hexagonal simulation cell was set to $(29.568 \times 29.568 \times 60.000) \text{ \AA}^3$. Periodic boundary conditions were applied in the three directions, but a large vacuum space along z was taken into account to avoid spurious interactions between replicas. After the surface optimization, the interlayer AA and BB distances were 6.865 and 6.867 \AA , respectively. During the optimizations, the HOPG bottom layer was kept fixed to bulk positions while the topmost ones were left free to relax in order to reproduce their surface-like behaviour. Geometry optimizations were performed using the BFGS algorithm and a convergence accuracy on nuclear forces of 4.5×10^{-5} Hartree Bohr⁻¹. A convergence threshold criterion on the maximum gradient of the wavefunction in the SCF procedure of 3×10^{-6} Hartree was used applying a Fermi–Dirac distribution with a broadening (electronic temperature) of 2500 K in order to facilitate the convergence. The Density of States (DOS) for each conformer extrapolated from the 1@HOPG optimized scenario were computed by performing single point calculations using a “revised” B3LYP functional, which includes an amount of 15% of the Hartree–Fock exchange, instead of the ordinary 20%. The computed DOS were convoluted with Gaussian functions with a full width half-maximum (FWHM, σ) of 0.6 eV.

Conflicts of interest

There are no conflicts to declare.

Acknowledgements

We acknowledge Synchrotrons staff and Peng Chen for the help given during beamtimes. M. M. K. is grateful to the Deutsche Forschungsgemeinschaft (DFG Research Grant KH 279/3) for financial support. PR and AN acknowledge the financial support of ANR-CHIOTS (no. ANR-11-JS07-013-01), CNRS, Université de Bordeaux and Région Nouvelle Aquitaine. The research leading to these results has received funding from the European Community's Seventh Framework Programme (FP7/2007–2013) under grant agreement no. 312284. L. P., F. T. and M. M. are grateful the European Research Council through the Advanced Grant 'MolNanoMas' (267746). L. P. F. T and M. M. acknowledge Fondazione Ente Cassa Risparmio di Firenze (SPIN-E m project cod. 2017.0730) and MIUR-Italy ("Progetto Dipartimenti di Eccellenza 2018–2022" allocated to Department of Chemistry "Ugo Schiff" and FIR Nanoplasmag project cod. RBFR10OAI0) for the economic support. The computing resources and the related technical support used for this work have been provided by CRESCO/ENEAGRID High Performance Computing infrastructure and its staff.⁵⁷ CRESCO/ENEAGRID High Performance Computing infrastructure is funded by ENEA, the Italian National Agency for New Technologies, Energy and Sustainable Economic Development and by Italian and European research programmes, see <http://www.cresco.enea.it/english> for information.

References

- 1 J. S. Moodera, B. Koopmans and P. M. Oppeneer, *MRS Bull.*, 2014, **39**, 578–581.
- 2 G. Molnár, S. Rat, L. Salmon, W. Nicolazzi and A. Bousseksou, *Adv. Mater.*, 2018, **30**, 1703862.
- 3 C. Lefter, V. Davesne, L. Salmon, G. Molnár, P. Demont, A. Rotaru and A. Bousseksou, *Magnetochemistry*, 2016, **2**, 18.
- 4 P. Gütllich and H. A. Goodwin, *Spin Crossover in Transition Metal Compounds I-III*, Springer Berlin Heidelberg, Berlin, Heidelberg, 2004, vol. 233–235.
- 5 M. A. Halcrow, *Spin-Crossover Materials: Properties and Applications*, John Wiley & Sons Ltd, Oxford, UK, 2013.
- 6 T. Miyamachi, M. Gruber, V. Davesne, M. Bowen, S. Boukari, L. Joly, F. Scheurer, G. Rogez, T. K. Yamada, P. Ohresser, E. Beaurepaire and W. Wulfhekel, *Nat. Commun.*, 2012, **3**, 938.
- 7 T. G. Gopakumar, M. Bernien, H. Naggert, F. Matino, C. F. Hermanns, A. Bannwarth, S. Mühlenberend, A. Krüger, D. Krüger, F. Nickel, W. Walter, R. Berndt, W. Kuch and F. Tucek, *Chem. – Eur. J.*, 2013, **19**, 15702–15709.
- 8 K. Bairagi, O. Iasco, A. Bellec, A. Kartsev, D. Li, J. Lagoute, C. Chacon, Y. Girard, S. Rousset, F. Miserque, Y. J. Dappe, A. Smogunov, C. Barreteau, M.-L. Boillot, T. Mallah and V. Repain, *Nat. Commun.*, 2016, **7**, 12212.
- 9 K. Bairagi, A. Bellec, C. Fourmental, O. Iasco, J. Lagoute, C. Chacon, Y. Girard, S. Rousset, F. Choueikani, E. Otero, P. Ohresser, P. Saintavit, M.-L. Boillot, T. Mallah and V. Repain, *J. Phys. Chem. C*, 2018, **122**, 727–731.
- 10 O. A. Scherman, G. B. W. L. Ligthart, R. P. Sijbesma and E. W. Meijer, *Angew. Chem., Int. Ed.*, 2006, **45**, 2072–2076.
- 11 T. G. Gopakumar, F. Matino, H. Naggert, A. Bannwarth, F. Tucek and R. Berndt, *Angew. Chem., Int. Ed.*, 2012, **51**, 6262–6266.
- 12 M. Bernien, D. Wiedemann, C. F. Hermanns, A. Krüger, D. Rolf, W. Kroener, P. Müller, A. Grohmann and W. Kuch, *J. Phys. Chem. Lett.*, 2012, **3**, 3431–3434.
- 13 A. Pronschinske, Y. Chen, G. F. Lewis, D. A. Shultz, A. Calzolari, M. B. Nardelli and D. B. Dougherty, *Nano Lett.*, 2013, **13**, 1429–1434.
- 14 A. Pronschinske, R. C. Bruce, G. Lewis, Y. Chen, A. Calzolari, M. Buongiorno-Nardelli, D. A. Shultz, W. You and D. B. Dougherty, *Chem. Commun.*, 2013, **49**, 10446–10452.
- 15 B. Warner, J. C. Oberg, T. G. Gill, F. El Hallak, C. F. Hirjibehedin, M. Serri, S. Heutz, M.-A. A. Arrio, P. Saintavit, M. Mannini, G. Poneti, R. Sessoli and P. Rosa, *J. Phys. Chem. Lett.*, 2013, **4**, 1546–1552.
- 16 X. Zhang, T. Palamarciuc, J.-F. Létard, P. Rosa, E. V. Lozada, F. Torres, L. G. Rosa, B. Doudin and P. A. Dowben, *Chem. Commun.*, 2014, **50**, 2255–2257.
- 17 E. Ludwig, H. Naggert, M. Källäne, S. Rohlf, E. Kröger, A. Bannwarth, A. Quer, K. Rosnagel, L. Kipp and F. Tucek, *Angew. Chem., Int. Ed.*, 2014, **53**, 3019–3023.
- 18 E. J. Devid, P. N. Martinho, M. V. Kamalakar, I. Šalitroš, Ú. Prendergast, J.-F. F. Dayen, V. Meded, T. Lemma, R. González-Prieto, F. Evers, T. E. Keyes, M. Ruben, B. Doudin and S. J. Van Der Molen, *ACS Nano*, 2015, **9**, 4496–4507.
- 19 M. Atzori, L. Poggini, L. Squillantini, B. Cortigiani, M. Gonidec, P. Bencok, R. Sessoli and M. Mannini, *J. Mater. Chem. C*, 2018, **6**, 8885–8889.
- 20 L. Poggini, M. Gonidec, J. H. González-Estefan, G. Pecastaings, B. Gobaut and P. Rosa, *Adv. Electron. Mater.*, 2018, **1800204**, 1800204.
- 21 L. Poggini, M. Gonidec, R. K. Canjeevaram Balasubramanyam, L. Squillantini, G. Pecastaings, A. Caneschi and P. Rosa, *J. Mater. Chem. C*, 2019, **7**, 5343–5347.
- 22 T. Knaak, C. González, Y. J. Dappe, G. D. Harzmann, T. Brandl, M. Mayor, R. Berndt and M. Gruber, *J. Phys. Chem. C*, 2019, **123**, 4178–4185.
- 23 L. Kipgen, M. Bernien, S. Ossinger, F. Nickel, A. J. Britton, L. M. Arruda, H. Naggert, C. Luo, C. Lotze, H. Ryll, F. Radu, E. Schierle, E. Weschke, F. Tucek and W. Kuch, *Nat. Commun.*, 2018, **9**, 1–8.
- 24 F. Schleicher, M. Studniarek, K. S. Kumar, E. Urbain, K. Katcko, J. Chen, T. Frauhammer, M. Hervé, U. Halisdemir, L. M. Kandpal, D. Lacour, A. Riminucci, L. Joly, F. Scheurer, B. Gobaut, F. Choueikani, E. Otero, P. Ohresser, J. Arabski, G. Schmerber, W. Wulfhekel, E. Beaurepaire, W. Weber, S. Boukari, M. Ruben and

- M. Bowen, *ACS Appl. Mater. Interfaces*, 2018, **10**, 31580–31585.
- 25 L. Poggini, M. Milek, G. Londi, A. Naim, G. Poneti, L. Squillantini, A. Magnani, F. Totti, P. Rosa, M. M. Khusniyarov and M. Mannini, *Mater. Horiz.*, 2018, **5**, 506–513.
- 26 M. Bernien, H. Naggert, L. M. Arruda, L. Kipgen, F. Nickel, J. Miguel, C. F. Hermanns, A. Krüger, D. Krüger, E. Schierle, E. Weschke, F. Tuzcek and W. Kuch, *ACS Nano*, 2015, **9**, 8960–8966.
- 27 S. Beniwal, X. Zhang, S. Mu, A. Naim, P. Rosa, G. Chastanet, J.-F. Létard, J. Liu, G. E. Sterbinsky, D. A. Arena, P. A. Dowben and A. Enders, *J. Phys.: Condens. Matter*, 2016, **28**, 206002.
- 28 X. Zhang, T. Palamarciuc, P. Rosa, J. F. Létard, B. Doudin, Z. Zhang, J. Wang and P. A. Dowben, *J. Phys. Chem. C*, 2012, **116**, 23291–23296.
- 29 X. Zhang, P. S. Costa, J. Hooper, D. P. Miller, A. T. N'Diaye, S. Beniwal, X. Jiang, Y. Yin, P. Rosa, L. Routaboul, M. Gonidec, L. Poggini, P. Braunstein, B. Doudin, X. Xu, A. Enders, E. Zurek and P. A. Dowben, *Adv. Mater.*, 2017, **29**, 1702257.
- 30 M. M. Khusniyarov, *Chem. – Eur. J.*, 2016, **22**, 15178–15191.
- 31 M.-L. Boillot, J. Zarembowitch and A. Sour, in *Spin Crossover in Transition Metal Compounds II*, ed. P. Gülich and H. A. Goodwin, Springer-Verlag Berlin Heidelberg, New York, 2004, pp. 261–276.
- 32 M. Milek, F. W. Heinemann and M. M. Khusniyarov, *Inorg. Chem.*, 2013, **52**, 11585–11592.
- 33 M. Mörtel, A. Witt, F. W. Heinemann, S. Bochmann, J. Bachmann and M. M. Khusniyarov, *Inorg. Chem.*, 2017, **56**, 13174–13186.
- 34 K. Uchida, Y. Nakayama and M. Irie, *Bull. Chem. Soc. Jpn.*, 1990, **63**, 1311–1315.
- 35 G. Poneti, L. Poggini, M. Mannini, B. Cortigiani, L. Sorace, E. Otero, P. Sainctavit, A. Magnani, R. Sessoli and A. Dei, *Chem. Sci.*, 2015, **6**, 2268–2274.
- 36 G. Poneti, M. Mannini, B. Cortigiani, L. Poggini, L. Sorace, E. Otero, P. Sainctavit, R. Sessoli and A. Dei, *Inorg. Chem.*, 2013, **52**, 11798–11805.
- 37 P. Totaro, L. Poggini, A. Favre, M. Mannini, P. Sainctavit, A. Cornia, A. Magnani and R. Sessoli, *Langmuir*, 2014, **30**, 8645–8649.
- 38 L. Poggini, G. Cucinotta, A.-M. Pradipto, M. Scarrozza, P. Barone, A. Caneschi, P. Graziosi, M. Calbucci, R. Cecchini, V. A. Dediu, S. Picozzi, M. Mannini and R. Sessoli, *Adv. Mater. Interfaces*, 2016, **3**(14), 1500855.
- 39 C. J. Powell and M. P. Seah, *J. Vac. Sci. Technol.*, A, 1990, **8**, 735–763.
- 40 Y. G. Borod'ko, S. I. Vetchinkin, S. L. Zimont, I. N. Ivleva and Y. M. Shul'ga, *Chem. Phys. Lett.*, 1976, **42**, 264–267.
- 41 G. Poneti, L. Poggini, M. Mannini, B. Cortigiani, L. Sorace, E. Otero, P. Sainctavit, A. Magnani, R. Sessoli and A. Dei, *Chem. Sci.*, 2015, **6**, 2268–2274.
- 42 J. Chastain and J. Moulder, *Handbook of X-ray photoelectron spectroscopy: a reference book of standard spectra for identification and interpretation of XPS data*, 1995.
- 43 N. Katsonis, T. Kudernac, M. Walko, S. J. van der Molen, B. J. van Wees and B. L. Feringa, *Adv. Mater.*, 2006, **18**, 1397–1400.
- 44 B. Rösner, M. Milek, A. Witt, B. Gobaut, P. Torelli, R. H. Fink and M. M. Khusniyarov, *Angew. Chem., Int. Ed.*, 2015, **54**, 12976–12980.
- 45 T. C. Pijper, O. Ivashenko, M. Walko, P. Rudolf, W. R. Browne and B. L. Feringa, *J. Phys. Chem. C*, 2015, **119**, 3648–3657.
- 46 S. M. Mendoza, M. Lubomska, M. Walko, B. L. Feringa and P. Rudolf, *J. Phys. Chem. C*, 2007, **111**, 16533–16537.
- 47 F. Nickel, M. Bernien, M. Herder, S. Wrzalek, P. Chittas, K. Kraffert, L. M. Arruda, L. Kipgen, D. Krüger, S. Hecht and W. Kuch, *J. Phys.: Condens. Matter*, 2017, **29**, 374001.
- 48 S. Tanaka, M. Toba, T. Nakashima, T. Kawai and K. Yoshino, *Jpn. J. Appl. Phys.*, 2008, **47**, 1215–1218.
- 49 J. Frisch, M. Herder, P. Herrmann, G. Heimel, S. Hecht and N. Koch, *Appl. Phys. A*, 2013, **113**, 1–4.
- 50 L. Malavolti, L. Poggini, L. Margheriti, L. Chiappe, P. Graziosi, B. Cortigiani, V. Lanzilotto, F. Buatier de Mongeot, P. Ohresser, E. Otero, F. Choueikani, P. Sainctavit, I. Bergenti, V. A. Dediu, M. Mannini and R. Sessoli, *Chem. Commun.*, 2013, **49**, 11506–11508.
- 51 L. Malavolti, V. Lanzilotto, S. Ninova, L. Poggini, I. Cimatti, B. Cortigiani, L. Margheriti, D. Chiappe, E. Otero, P. Sainctavit, F. Totti, A. Cornia, M. Mannini and R. Sessoli, *Nano Lett.*, 2015, **15**(1), 535–541.
- 52 P. Gülich and H. A. Goodwin, *Spin Crossover in Transition Metal Compounds II*, Springer Berlin Heidelberg, Berlin, Heidelberg, 2004, vol. 234.
- 53 L. Kipgen, M. Bernien, F. Nickel, H. Naggert, A. J. Britton, L. M. Arruda, E. Schierle, E. Weschke, F. Tuzcek and W. Kuch, *J. Phys.: Condens. Matter*, 2017, **29**, 394003.
- 54 M. Nishino, K. Boukheddaden, Y. Konishi and S. Miyashita, *Phys. Rev. Lett.*, 2007, **98**, 1–4.
- 55 G. Félix, W. Nicolazzi, M. Mikolasek, G. Molnár and A. Bousseksou, *Phys. Chem. Chem. Phys.*, 2014, **16**, 7358.
- 56 W. Nicolazzi and A. Bousseksou, *C. R. Chim.*, 2018, **21**, 1060–1074.
- 57 G. Ponti, F. Palombi, D. Abate, F. Ambrosino, G. Aprea, T. Bastianelli, F. Beone, R. Bertini, G. Bracco, M. Caporicci, B. Calosso, M. Chinnici, A. Colavincenzo, A. Cucurullo, P. Dangelo, M. De Rosa, P. De Michele, A. Funel, G. Furini, D. Giammattei, S. Giusepponi, R. Guadagni, G. Guarnieri, A. Italiano, S. Magagnino, A. Mariano, G. Mencuccini, C. Mercuri, S. Migliori, P. Ornelli, S. Pecoraro, A. Perozziello, S. Pierattini, S. Podda, F. Poggi, A. Quintiliani, A. Rocchi, C. Scio, F. Simoni and A. Vita, in *2014 International Conference on High Performance Computing & Simulation (HPCS)*, IEEE, 2014, pp. 1030–1033.
- 58 D.-Q. Yang and E. Sacher, *Langmuir*, 2006, **22**, 860–862.
- 59 J. J. Yeh and I. Lindau, *At. Data Nucl. Data Tables*, 1985, **32**, 1–155.
- 60 P. Ohresser, E. Otero, F. Choueikani, K. Chen, S. Stanescu, F. Deschamps, T. Moreno, F. Polack, B. Lagarde,

- J.-P. Daguerre, F. Marteau, F. Scheurer, L. Joly, J.-P. Kappler, B. Muller, O. Bunau and P. Saintavit, *Rev. Sci. Instrum.*, 2014, **85**, 013106.
- 61 J. Hutter, M. Iannuzzi, F. Schiffmann and J. Vandevondele, *Wiley Interdiscip. Rev.: Comput. Mol. Sci.*, 2014, **4**, 15–25.
- 62 C. Lee, W. Yang and R. G. Parr, *Phys. Rev. B: Condens. Matter Mater. Phys.*, 1988, **37**, 785–789.
- 63 A. D. Becke, *Phys. Rev. A*, 1988, **38**, 3098–3100.
- 64 Y. Zhang and W. Yang, *Phys. Rev. Lett.*, 1998, **80**, 890.
- 65 R. Sabatini, T. Gorni and S. de Gironcoli, *Phys. Rev. B: Condens. Matter Mater. Phys.*, 2013, **87**, 041108.
- 66 E. F. Pettersen, T. D. Goddard, C. C. Huang, G. S. Couch, D. M. Greenblatt, E. C. Meng and T. E. Ferrin, *J. Comput. Chem.*, 2004, **25**, 1605–1612.